ingegneria sismica
International Journal of Earthquake Engineering
Anno XLIII - Num. 1 - 2026

Research and application of mobile anti-falling technology for aerial work in power grid

Jun Zhang[1], *Pengtian Huang*[2,*], *Hao Yu*[1], *Lisha Zhang*[2] *and Bin Ma*[1]

[1] Qinghai Power Transmission and Transformation Engineering Company, Xining, Qinghai, 810001, China
[2] State Grid Yushu Power Supply Company, Yushu, Qinghai, 815000, China

SUMMARY: *In the construction process of power industry, there are many high-altitude operations, and the high-altitude fall prevention technology and device is an important guarantee for the personal safety of electric power operators. The UAV-mounted fall prevention device in the power grid aerial work greatly avoids the risk of high-altitude personal fall accidents. The device is based on visual SLAM algorithm to realize target localization, and based on PID algorithm to complete attitude control. Simulation test results show that the ORB-SLAM2 algorithm with multi-sensors improves the system localization accuracy by about 21.4% compared with the ORB-SLAM algorithm that only supports monocular camera. The UAV can achieve attitude stabilization under the PID-based attitude controller when carrying different loads, but some oscillations will occur when the weight of the carried load reaches 15 kg or the load is seriously asymmetric. Based on UAV technology, the high-altitude operation method of power grid can effectively eliminate the potential hidden dangers brought by the inconvenient use of the current temporary fall protection measures and thus affect the coherence of the tower boarding action, and at the same time, it can realize the fall protection in the whole process of tower boarding, which can effectively alleviate the psychological pressure of the boarding personnel and reduce the risk of falling.*

KEYWORDS: *SLAM algorithm; PID algorithm; unmanned aerial vehicle; high-altitude fall protection*

1 Introduction

Power grid work-at-height refers to the construction activities at height in and around power facilities, which may involve power towers, power lines, substations and other facilities [1, 2]. The role of mobile fall protection technology for work-at-height is mainly to prevent the workforce from falling from height and to protect their personal safety [3]. In the process of power grid operation at height, the operators usually need to stand on the power tower or pole to carry out a variety of operations, such as installation, maintenance, overhaul and so on [4, 5]. Due to the high operating height, once a fall accident occurs, the consequences will be unimaginable. Therefore, the role of mobile fall protection safety technology for power grid operation at height is to utilize safety equipment and measures with mobility to prevent operators from falling from height [6, 7].

Common mobile fall prevention techniques include safety belt systems and aerial lifting baskets. The harness system is the basic solution to prevent falls from height on the power grid.

*Huangpt2025@163.com
https://doi.org/10.65102/is2026033
Published: 30 April, 2026

It usually consists of a safety belt, a safety belt pulley, a space bar, a wire rope, a control valve, a safety belt connector, a fixing hook, etc. The operator wears the safety belt connector and fixes it to the fixing hook, and the wire rope is bound to the fixing point through the pulley [8-11]. During the operation, the safety belt can slide freely to ensure the safety of the operator. When the operators fall from height or lose balance, the safety belt system can quickly intercept them, thus avoiding fall accidents [12, 13]. Aerial gondola is a commonly used equipment for overhead work on power grids, which can safely and efficiently carry out maintenance, overhauling and upgrading of power facilities [14]. The aerial cradle usually consists of the cradle body, connecting rods, hydraulic system, and safety devices, etc. The cradle itself can be lifted, rotated, and moved so that the operator can easily reach the place where the work needs to be done [15, 16]. At the same time, various safety devices, such as limit switches, restriction ropes, and self-rescue devices, are installed on the cradle to ensure the safety of the operators.

This paper explores the working principle of UAV mounted fall arrest device from two aspects: target localization and attitude control. Based on the ROS platform, the effectiveness of the ORB-SLAM2 algorithm is verified on the KITTI dataset. The UAV attitude Simulink control structure based on PID control is built in MATLAB/Simulink environment, and the attitude tracking simulation experiments are designed for the UAV carrying asymmetric loads, symmetric loads, large weight asymmetric loads and severe asymmetric loads. Based on the tracking desired attitude angle signals of UAV roll angle, pitch angle and yaw angle, the control effect of PID algorithm is examined. The application of UAV-mounted fall prevention device makes the safety coefficient of power grid aerial operation greatly improved, and promotes the generation of safer, more convenient and quicker way of ascending.

2 Technical research on drone-mounted fall arrest devices

The drone mounting device can transport the equipment to the designated working height and guarantee the precise installation in place. The working principle and fall prevention principle of the drone mounted device are shown in Fig. 1 and Fig. 2 respectively. The UAV carries the tower protection fixed bracket and security rope to the top of the tower, and utilizes the self-locking mechanism of the fixed bracket to realize the rapid installation and removal of the fixed bracket at the top of the tower with the assistance of real-time video transmission. One end of the security rope is fixed in the tower protection fixed bracket, and the other end is fixed at the bottom of the tower, and the fall arrester is connected with the security rope to form a complete protection measure, which can effectively guarantee the safety of the tower climbers.

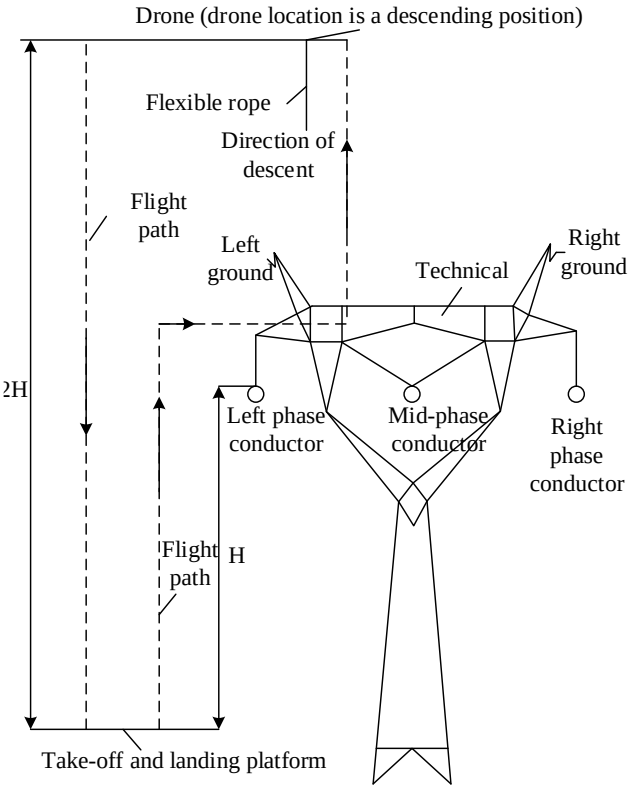

Figure 1: The working principle of a drone mount

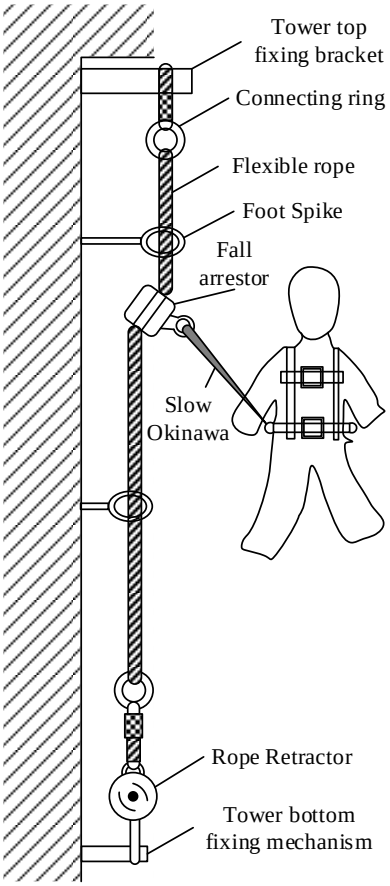

Figure 2: The unmanned device is a device that prevents falling

The drone mounted device realizes the aerial transportation and precise positioning of the device with the help of the flight characteristics of the drone, which improves the efficiency and flexibility of the power grid's high-altitude operation. In terms of positioning, it mainly relies on visual recognition technology, specifically, the image captured by the camera is used to determine the relative position between the drone and the tower. Subsequently, a feedback PID control algorithm is applied, and the controller is utilized to ensure that the UAV flies smoothly and accurately arrives at the marked target location.

2.1 Visual SLAM-based target localization implementation

SLAM refers to the simultaneous localization and mapping technique, where localization means that a matching algorithm estimates the current position and attitude information using the detected features of the environment, and mapping builds a map of the current environment based on the estimated position and attitude information.

2.1.1 Camera Model and Projection Matrix

In the field of computer vision, a camera sensor is first needed to convert the information in three-dimensional space into the form of a two-dimensional photo, and then the photo is processed by an algorithm to obtain information such as the movement state. Among the camera models used to transform 3D spatial information into 2D state information, the most common is the camera projection model. According to the principle of small hole imaging, an object P in the real world passing through a pinhole will form a reflection on the projection plane, and the camera projection model is shown in Figure 3.

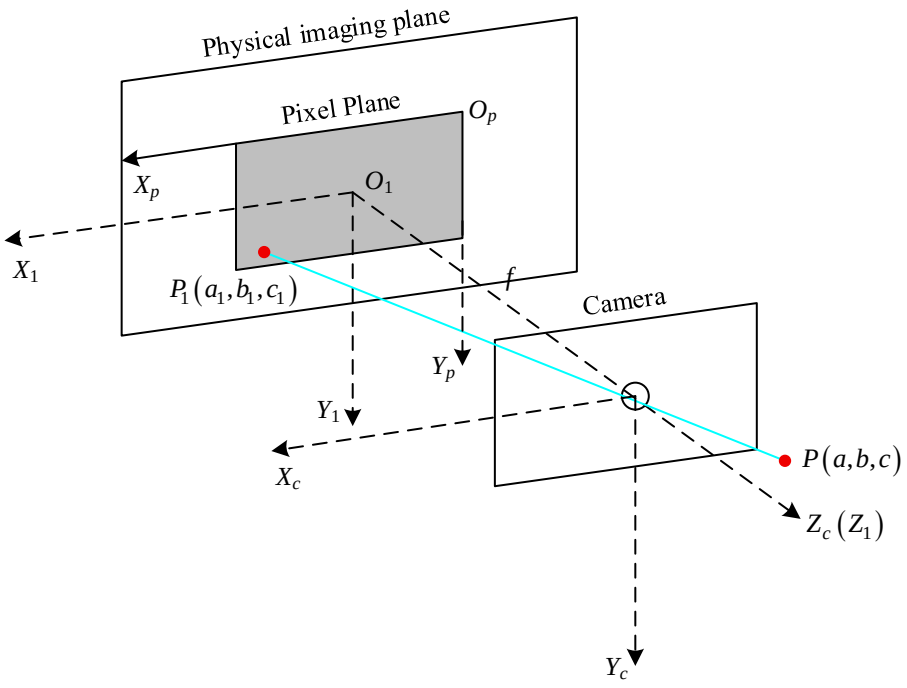

Figure 3: Camera projection model

Suppose there is a point $P(a,b,c)$ in three-dimensional space, and this point is projected onto the camera plane to produce the pixel point $P_1(a_1,b_1,c_1)$ Assuming that the distance of the camera plane from the optical center is c_1, then the projection equation can be expressed

as shown in equation (1):

$$\frac{a_1}{a}=\frac{b_1}{b}=\frac{c_1}{c} \tag{1}$$

Eq. (2) can be obtained by converting Eq. (1) into matrix form:

$$z*\begin{bmatrix}u\\v\\i\end{bmatrix}=\begin{bmatrix}x\\y\\z\end{bmatrix}\rightarrow z*p=X \tag{2}$$

In equation (2), z denotes the depth value of p. Denoted by C, combined with Eq. (2), the projection equation can be written as Eq. (3):

$$zp=CX, C=\begin{bmatrix}f_x & 0 & c_x\\0 & f_y & c_y\\0 & 0 & 1\end{bmatrix} \tag{3}$$

Considering that the camera is in motion at all times during the movement of the UAV, the specific motion can be categorized into three-dimensional rotation and displacement, with the matrix R to represent the three-dimensional rotation, and T to represent the displacement, the projection equation can be expressed in the form shown in equation (4):

$$zp=C(RX+T) \tag{4}$$

Eq. (4) describes the projection equation in the motion environment, where the internal reference C can be obtained after calibrating the camera, p can be observed in the image, while z, X, R are the variables to be estimated, and X is the total trajectory of the camera during the motion.

2.1.2 Visual SLAM realization process

The general process of vision SLAM is shown in Fig. 4. In ORB-SLAM, the process shown in Fig. 4 can be corresponded to three parts: feature point extraction and matching, BA and optimization, and loopback detection.

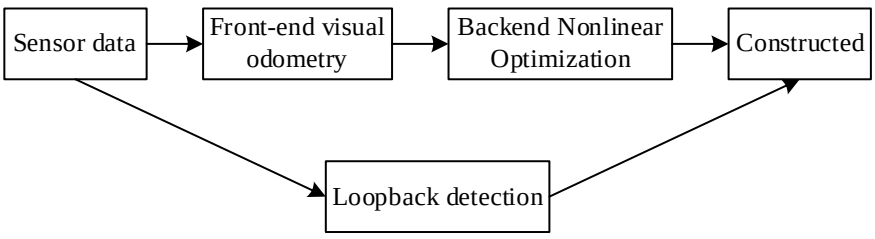

Figure 4: Visual SLAM data processing process

(1) Feature point extraction and matching

The information contained in the feature points in each image has key points as well as descriptors. The real-time nature of feature extraction mainly depends on the computational

capability of the processor, and considering the performance compromise between the two, ORB-SLAM is undoubtedly the optimal program.

In the ORB feature extraction process, the information contained in the feature points is also called ORB features. Its extraction process mainly contains two steps. FAST corner point extraction and BRIEF descriptor, respectively.

Firstly, FAST corner point extraction is carried out, defining the moments of a small image block as m_{pq}, and the specific process is shown in equation (5):

$$m_{pq} = \sum_{x,y \in B} x^p y^q I\left(x \quad y\right), p, q = \left\{0 \quad 1\right\} \tag{5}$$

The center of gravity of this image block can be found by Eq. (1), as shown in Eq. (6):

$$C = \left(\frac{m_{10}}{m_{00}} \quad \frac{m_{01}}{m_{00}} \right) \tag{6}$$

Then the line between the center position O and the center of gravity C of this image block is $\overrightarrow{OC}$, then the direction of the feature point can be found, as shown in equation (7):

$$\theta = \arctan\left(m_{01} / m_{10}\right) \tag{7}$$

The scale and rotation information can be obtained through the above process, and the next step is to compute the descriptor corresponding to the feature point, which is described in ORB-SLAM using the optimized BRIEF approach. By comparing the size of two neighboring pixels to assign a value of 0 or 1, if the image block contains 135 pixel points, then the descriptor of the image block is a vector of 0 or 1 in 135 dimensions.

The process of feature matching is also the process of finding the correlation between images. Assuming that the feature points of two images are $x_t^m, m = 1, 2M$ and $x_{t+1}^n, n = 1, 2N$, the matching is done in a violent way, i.e., calculating the degree of similarity in the two images, and then the results are ranked, and the two points with the smallest value are considered to be matched successfully. The distance is computed in ORB-SLAM using Hamming's formula, while Hamming's distance is a conceptual description and does not represent the distance information between two points, but rather the number of two binary numbers with different corresponding bits.

(2) BA and Optimization

BA optimization refers to the process of refining the optimal 3D model as well as the camera parameters from the visual reconstruction, where a realistic point p is projected to the pixel coordinates as an observation equation, which can be written in the form shown in Eq. (8):

$$z = h(x, y) \tag{8}$$

In Eq. (8), x represents the camera's positional information, including rotation R and translation t, and the corresponding Lie algebra ζ, y is the positional information of p in the world coordinate system, then the error of this observation can be expressed as Eq. (9):

$$e = z - h(\zeta p) \tag{9}$$

Considering the error of historical moments, then the overall cost function can be expressed

as shown in equation (10):

$$\frac{1}{2}\sum_{i=1}^{m}\sum_{j=1}^{n}\left\|e_{ij}\right\|^2=\frac{1}{2}\sum_{i=1}^{m}\sum_{j=1}^{n}\left\|z_{ij}-h\left(\zeta_i p_j\right)\right\|^2 \tag{10}$$

Equation (10) can be solved to adjust and optimize the position and road marking.

(3) Loopback detection

For how to determine that the robot moves to the same location, ORB-SLAM introduces the bag-of-words model and dictionary concept. The bag-of-words model represents the size of the ratio of the number of features in each node to the overall number of features, assuming that there exists a node with a total number of features of n, and its total number of features is n_i, then the IDF of the word is shown in equation (11):

$$IDF_i=\log\frac{n}{n_i} \tag{11}$$

In addition, TF denotes the frequency of occurrence of a feature in an image, assuming that the word w_i is displayed in a certain image with a frequency of n_i and the total number of words is n, then the TF can be expressed as shown in equation (12):

$$TF_i=\frac{n_i}{n} \tag{12}$$

Then, the weight η_i of w_i can be calculated by equation (12):

$$\eta_i=TF_i\times IDF_i \tag{13}$$

Combined with the weights, the bag-of-words model for this image can be expressed as equation (14):

$$A=\left\{\left(w_1\quad\eta_1\right)\left(w_2\quad\eta_2\right)\left(w_N\quad\eta_N\right)\right\}v_A \tag{14}$$

The model can represent the images. Then the differences between the images can be represented in the form of a paradigm as shown in equation (15):

$$s\left(v_A-v_B\right)=2\sum_{i=1}^{N}\left|v_{Ai}\right|+\left|v_{Bi}\right|-\left|v_{Ai}-v_{Bi}\right| \tag{15}$$

Up to this point it is possible to calculate the similarity in the image by bag-of-words model.

For the implementation of visual SLAM algorithm, this paper considers from the situation that there are angular deviation and fast flight speed in the actual flight of UAV, and finally determines to choose to use the ORB-SLAM2 algorithm.ORB-SLAM2 algorithm compares with the ORB-SLAM algorithm, and the sensor upgrades from only supporting monocular camera to supporting monocular, binocular and RGB-D camera.

2.2 Attitude control based on PID algorithm

PID control is a kind of feedback loop control, including proportional coefficient P, integral

coefficient I and differential coefficient D, which correspond to the current error, cumulative error and future error, respectively.PID will be the difference between the input target value and the actual output of the proportional, integral, and differential processing, and then linearly combined together, to achieve feedback control. Its formula is:

$$u(t) = K_p\left[e(t) + \frac{1}{T_i}\int_0^t e(t)dt + \frac{T_d de(t)}{dt}\right] \tag{16}$$

A typical single-stage PID controller structure is shown in Figure 5. One of the main jobs of the flight control is the flight attitude correction to overcome the attitude abnormality caused by the installation of the vehicle, wear and tear of the devices, inconsistency between parts and external interference. When the deviation of the attitude value from the desired value is detected by accelerometers, gyroscopes and other inertial elements, the correction of the flight attitude is realized by PID control.

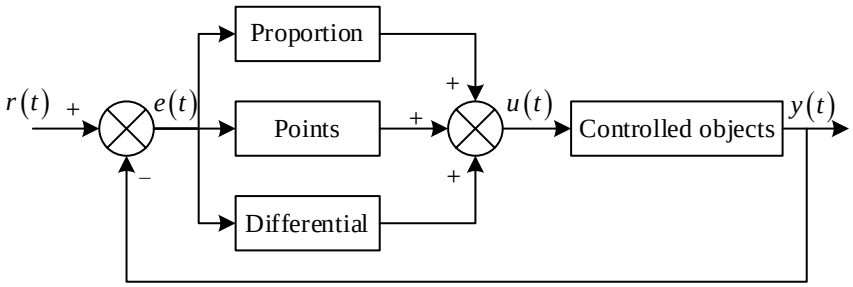

Figure 5: PID controller structure diagram

The proportionality coefficient P is used to generate the response speed. when the value of P is too small, the response speed is slow and it is difficult to realize the timely adjustment of the flight attitude, and when the value of P is too large, it will generate the oscillation, which affects the smooth flight of the quadrotor.

Integral coefficient I is used to eliminate the deviation and improve the control accuracy, and at the same time, the response speed can be improved on the basis of P.

The differential coefficient D is used to suppress the overshoot response and reduce the oscillation of P. Too large a value of D will slow down the response speed.

The pitch angle is controlled by PID, setting θ as the current pitch angle, θ_e as the desired pitch angle, and K_p, K_i, K_d as the proportional, integral, and differential gains, respectively, and the output of the PID control of pitch angle is:

$$\theta_o = K_p\Delta\theta(t) + K_i\int_0^t \Delta\theta(t)dt + K_d\Delta\theta(t) \tag{17}$$

where $\Delta\theta(t) = \theta_e - \theta$.

The roll angle is controlled by PID, setting φ as the current roll angle, φ_e as the desired roll angle, and the PID control output of the roll angle is:

$$\varphi_o = K_p\Delta\varphi(t) + K_i\int_0^t \Delta\varphi(t)dt + K_d\Delta\varphi(t) \tag{18}$$

where $\Delta\varphi(t) = \varphi_e - \varphi$.

The heading angle is controlled by PI, setting ψ as the current heading angle and ψ_c as the desired heading angle, and the PI control output of the heading angle is:

$$\psi_o = K_p \Delta\psi(t) + K_i \int_0^t \Delta\psi(t)dt \tag{19}$$

3 Processes for the application of fall arrest methods based on drone technology

3.1 Preparation for take-off

First, check the battery power, make sure the battery power of the drone and RC expansion is more than 85%. The second is to check the structure of the drone, to ensure that the arm is fully expanded and the arm snap is firmly fixed, the drone tripod installation is completed and firmly fixed, and the drone paddles are fully open. The third is to check the function of the UAV to ensure that the remote control of the UAV is connected normally, the remote control shows that the self-test of the UAV does not report any error, the remote control real-time dynamic carrier phase differential technology function is normal, the lower lighting function switch of the UAV can be opened and closed normally, and the definition of the UAV's remote control rocker is normal. Fourth, check the lower part of the UAV's obstacle avoidance to make sure that the obstacle avoidance is closed in case the landing operation cannot be carried out. Fifth, confirm that the function of the thrower is normal. Sixth, confirm that the UAV end visualization multi-joint flexible carrier is connected with the tower protection fixed bracket, security rope and the servo on the aircraft.

3.2 Fly-hanging operations

Control the UAV to fly to the designated location for the placement of the hook device, and when the hook is mounted and stuck in place, operate the UAV to descend so that it is detached from the fixed bracket hook, and take a picture of the hook stuck in place through the UAV to confirm that the device has been stuck securely, that is, to complete the fly-hanging operation. When the UAV carries the end visualization multi-joint flexible carrier back and approaches the ground, turn on the downward looking probe light of the UAV through the remote control to open the thrower pin, detach the end visualization multi-joint flexible carrier from the UAV, and then land the UAV normally after detachment.

3.3 Security rope fixing

With the climbing tower after completing the installation of the tower protection fixed bracket, the ground staff will fix one end of the security rope to the tower leg and install the fall arrester. The construction personnel will be the safety belt and tower security rope through the speed difference of high-altitude fall arrest self-locking device connected firmly, by the safety officer to check to confirm that all parts of the connection is reliable, the construction personnel can carry out climbing tower ascending operation.

3.4 Fixed bracket removal

By controlling the drone to fly to the designated location for the device's grasping action, the operator observes the visualization of the carrier hook at the drone end through the ground-side

image monitoring assistance system and connects it with the fixed bracket hook, then operates the drone to fly vertically upward, so that the fixed bracket can be separated from the tower and return to the ground.

4 Simulation testing

4.1 Experimental design

ROS is an open-source, free robotics operating system that can run on computer platforms, and it provides a series of programs and tools to help researchers develop and test robotics algorithms. Currently, it is mainly used in the research of autonomous algorithms for mobile robots, robotic arms, and unmanned aerial vehicles, and it provides a visual interface for researchers to intuitively display the robot's movements.

The study is based on the ROS platform and simulation experiments of localization algorithms on the KITTI dataset. The UAV attitude controller based on PID control is built in the Simulink environment of MATLAB, and a set of PID control parameters of each channel is integrated and rectified by using offline rectification of the parameters to test the effect of different loads on the attitude of the UAV.

The special sequence scene in the KITTI dataset 08. This sequence is the data captured near the high-voltage pylons under different environments of the carrier, and the sequence contains two major influencing factors, namely, different environments (daytime and nighttime) and high-voltage pylons' site points at the same time.

In this paper, the absolute trajectory error (APE) is used to evaluate the trajectory accuracy of the ORB-SLAM2 algorithm, and let the camera position computed by the algorithm at moment i be X_i, and the true position be $X_{t,i}, X_i, X_{t,i} \in SE(3)$, and the absolute trajectory error at the ith moment is:

$$APE\left(X_i, X_{t,i}\right) = X_{t,i}^{-1} X_i \tag{20}$$

The mean, variance, etc., can then be used to calculate all errors over the running time of the algorithm, and the root-mean-square error of the displacement is usually used to estimate the accuracy of the algorithm in generating trajectories:

$$RMSE(APE) = \left(\frac{1}{m} \sum_{i=1}^{m} \left\| trans\left(APE_i\right) \right\|^2 \right)^{\frac{1}{2}} \tag{21}$$

The *trans* in the formula indicates the trajectory error part of the position error between the real value and the predicted value, ignoring the perspective error.

After a series of trial cobbling of PID control parameters and comparison of experimental effects, the selected PID parameters for roll, pitch and yaw are as follows:

(1) Roll angle PID control: $K_P = 75, K_I = 0.05, K_D = 25$

(2) Pitch angle PID control: $K_P = 70, K_I = 0.05, K_D = 20$

(3) Yaw angle PID control: $K_P = 35, K_I = 0.01, K_D = 15$

Under the above PID controller parameters, to verify the effectiveness and robustness of the UAV attitude controller based on PID control.

4.2 Targeting Effectiveness Analysis

This paper compares the performance of the ORB-SLAM algorithm with the algorithm of this paper on the datasets. Among them, the algorithm of this paper selects the more typical 4 sets of data (ORB-SLAM2-1~ORB-SLAM2-4) in the results after multiple runs, and the test data are shown in Figure 6. Compared with ORB-SLAM, the algorithm in this paper improves the system accuracy by about 21.4%, and in the better case, it can reach 27.8%. Meanwhile, the algorithm in this paper optimizes the maximum error, average error, median error, and minimum error to different degrees. Especially for the minimum error, the enhancement can reach 71.6% in the better case.

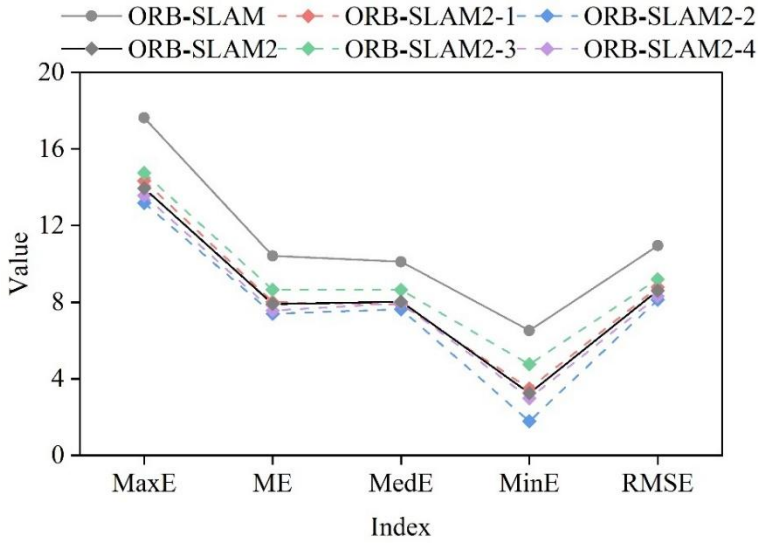

Figure 6: Test data for special scenarios

The ground truth trajectory comparison is shown in Fig. 7, (a) and (b) denote the ground truth trajectories of ORB-SLAM and this paper's algorithm, respectively. It can be seen that this paper's algorithm has significantly optimized the trajectory estimation bias and stability.

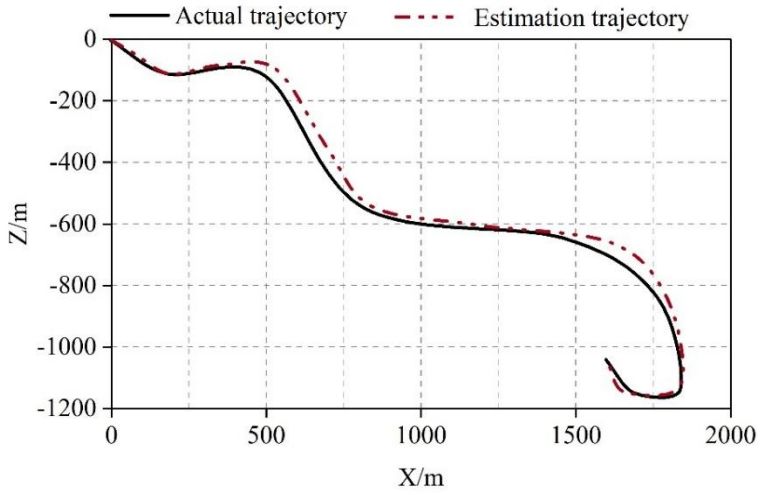

(a) ORB-SLAM

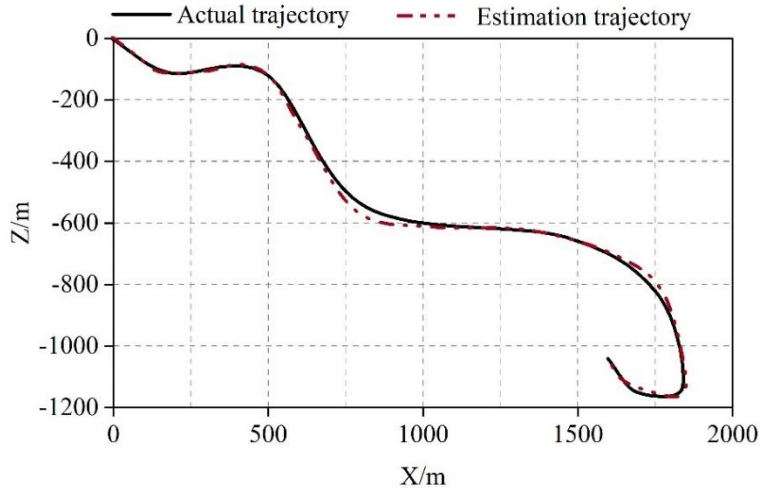

(b) ORB-SLAM2

Figure 7: The actual trajectory is compared to the estimated trajectory

4.3 Attitude control effect analysis

4.3.1 Effect of carrying asymmetric loads on UAV attitude

In the established control structure, set the load carried by the unmanned aerial vehicle as an asymmetric load, that is: The load weight was 8kg, and the carrying positions (x,y,z) were (0.05m,0.05m,1m). Under this condition, simulation experiments were conducted, and the experimental results are shown in Figure 8. (a) to (c) respectively represent the PID control results of roll Angle, pitch Angle, and yaw Angle (the same below). As can be seen from the figure, when the UAV carries the above asymmetric loads, the UAV roll angle, pitch angle and yaw angle can track the desired attitude angle signal well, with only a very small overshoot, which is within the allowable range. The comprehensive analysis shows that the UAV attitude controller based on PID control has good control effect in the case of UAV carrying asymmetric loads.

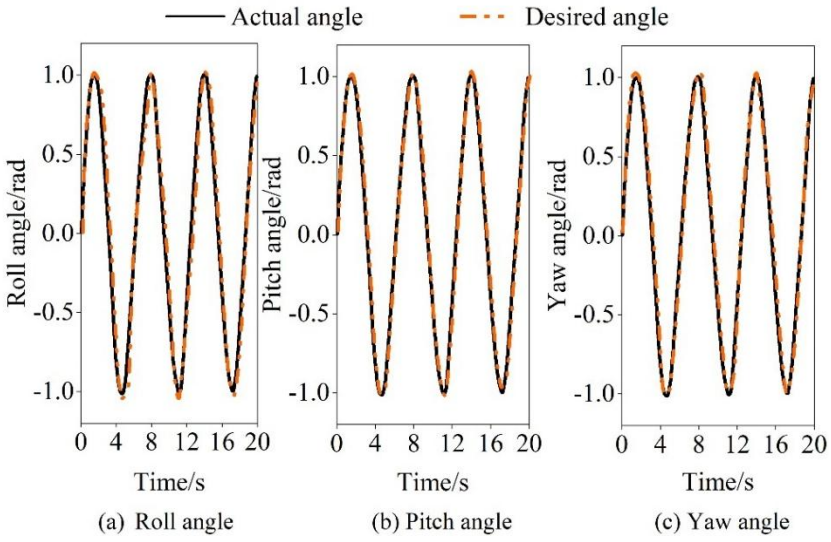

Figure 8: The impact of asymmetric loads on drone posture

4.3.2 Effect of carrying a symmetric payload on UAV attitude

The load carried by the UAV is set as a symmetric load in the built control structurer, i.e., the weight of the load is 8kg, and the carrying position (x,y,z) is (0m,0m,1m), and simulation experiments are carried out in this case, and the experimental results are obtained as shown in Fig. 9. From the figure, it can be seen that when the UAV carries the above symmetric load, the UAV roll angle, pitch angle and yaw angle can track the desired attitude angle signals well, and the overshooting is very small and can be ignored, which is better compared with the case when the UAV carries the asymmetric load in 4.3.1. From this, it can be inferred that the asymmetric load has more influence on the UAV attitude. The comprehensive analysis shows that the UAV attitude controller based on PID control has good control effect in the case of UAV carrying symmetric load.

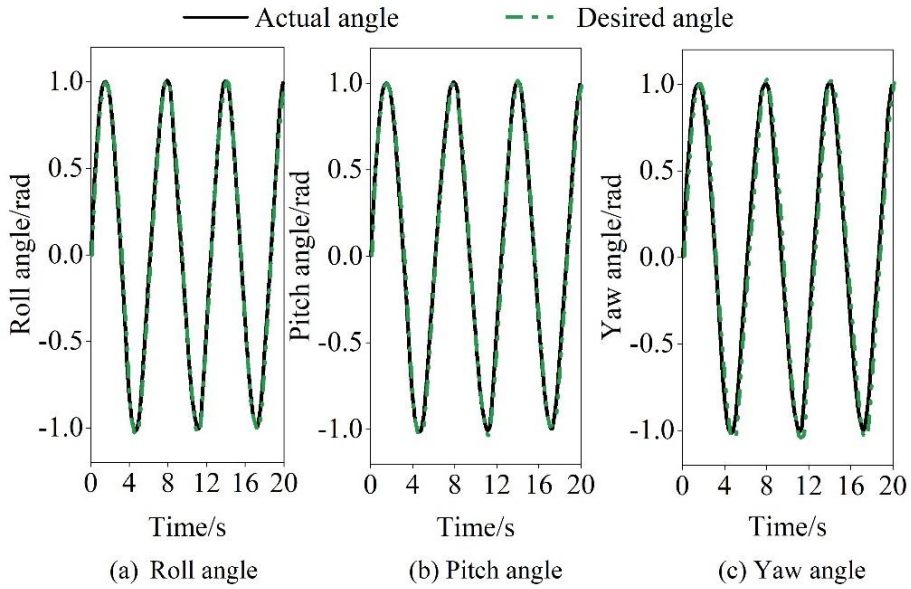

Figure 9: The effect of symmetrical load on drone posture

4.3.3 Effect of carrying large weight loads on UAV attitude

The load carried by the UAV is set to be a large weight asymmetric load in the built control structurer, i.e., the weight of the load is 15kg, and the carrying position (x,y,z) is (0.05m,0.05m,1m), and simulation experiments are carried out in this case, and the experimental results are obtained as shown in Fig. 10. As can be seen from the figure, when the UAV carries the above mentioned large weight asymmetric type load, the UAV roll angle, pitch angle and yaw angle can also track the desired attitude angle signal eventually, but it can be clearly seen that the effect is slightly worse compared with the experimental results in 4.3.1. This shows the effect of load mass on UAV attitude, while Figure (c) shows that large weight load has the least effect on yaw, which is in line with practical common sense. Comprehensive analysis shows that the UAV attitude controller based on PID control has a better control effect in the case of UAV carrying large-weight asymmetric loads, but there are shortcomings, which need to further improve the robustness of the controller.

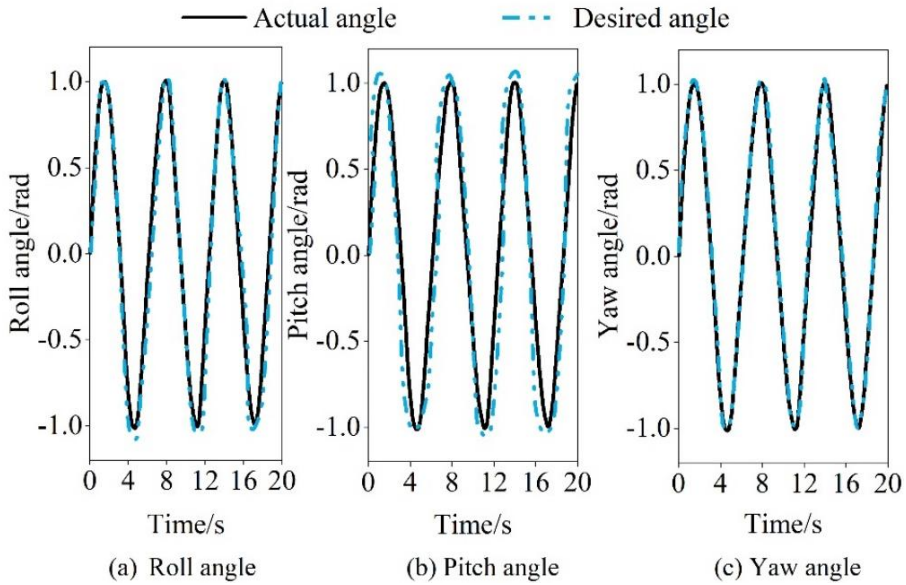

Figure 10: The impact of large weight load on drone posture

4.3.4 Effect of carrying a grossly asymmetric load on UAV attitude

The load carried by the UAV is set to be a severely asymmetric load in the built control structurer, i.e., the weight of the load is 8 kg, and the carrying position (x,y,z) is (1m,1m,1m), and simulation experiments are carried out in this case, and the experimental results are obtained as shown in Fig. 11. The load selected in this experiment is a more extreme case, i.e., severe asymmetry. In this case, the effect of UAV roll angle, pitch angle and yaw angle in tracking the desired attitude angle is more general, with overshooting and a certain amplitude of oscillation. Comprehensive analysis shows that the severe asymmetric load has a great influence on the UAV attitude, and under the control of the UAV attitude controller based on PID control, the UAV attitude can be stabilized, but there will be overshooting and oscillation, and the control effect needs to be improved.

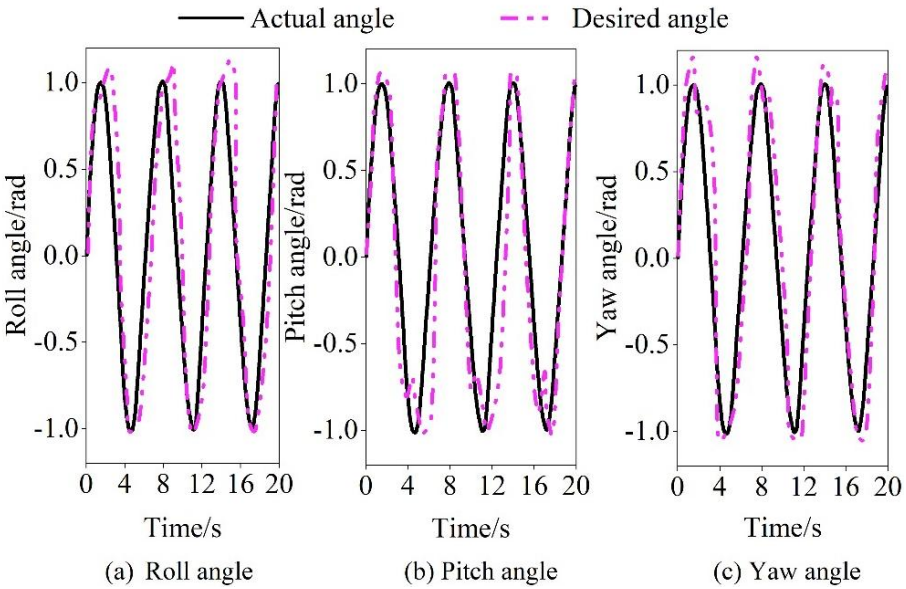

Figure 11: The impact of the load on drone posture is seriously incorrect

In summary, based on simulation tests, the target localization algorithm involved in the UAV-mounted fall prevention device can achieve accurate localization of the device in the air. The UAV attitude controller based on PID control can guarantee the smoothness of the device under non-extreme and normal weight loads.

5 Conclusion

The UAV mounted device is based on the target position estimated by the vision algorithm of ORB-SLAM2, and the PID control algorithm is applied to ensure the smooth flight of the UAV. The study verifies after simulation tests that the ORB -SLAM2 algorithm is more capable of improving the positioning accuracy by about 21.4% compared to the ORB -SLAM algorithm. The attitude controller based on PID control can ensure the flight stability under normal load conditions. The application process of the UAV mounted fall prevention device includes the steps of pre-takeoff preparation, fly-hanging operation, security rope fixation and fixed bracket removal. It realizes the whole process of “visualization+automation” for fall prevention, effectively protects the safety of tower climbers, and can be applied to power grid aerial work.

In this paper, the research on mobile fall prevention technology for power grid aerial work has good control effect in simulation experiments, but it has not been applied to the actual flight experiments of the UAV prototype. In the future research work, it is necessary to apply the trajectory tracking controller to the actual UAV, so as to more strongly prove the effectiveness of the controller in this paper.

Funding

This work was supported by the science and technology project of State Grid Corporation of China (Contract No.: 522824240002); Project name: Research, development and application of a full - process safety protection system for high - altitude operations.

About the Author

Jun Zhang was born in 1975 in Ledu, Qinghai province, China. He received a bachelor's degree from Qinghai University, China. Now, he works in Qinghai Power Transmission and transformation Engineering Company, and his research direction is the construction management of power transmission and transformation projects.

Pengtian Huang was born in Gansu, China in 1992. He works in Yushu Power Supply Company of State Grid. My research direction is the research and application of mobile anti-falling technology for high-altitude operation of power grid.

Hao Yu was born in Haidong, Qinghai Province, China in 1992. He received his bachelor's degree from Qinghai University, China. Now he is working in Qinghai Power Transmission and Transformation Engineering Co., Ltd., and his research direction is construction management of power transmission and transformation projects.

Lisha Zhang was born in Shaanxi, China in 1992. She works in the State Grid Yushu Power Supply Company. My research direction is the research and application of mobile anti-fall technology for high-altitude operation of power grid.

Bin Ma was born in Minhe, Qinghai, China, in 1975. Graduated from Xi'an University of Posts and Telecommunications in China with a bachelor's degree, he is currently working in Qinghai Power Transmission and Transformation Engineering Co., Ltd., mainly focusing on transmission line operation and maintenance management.

References

[1] Alvarez-Alvarado, M. S., Donaldson, D. L., Recalde, A. A., Noriega, H. H., Khan, Z. A., Velasquez, W., & Rodriguez-Gallegos, C. D. (2022). Power system reliability and maintenance evolution: A critical review and future perspectives. Ieee Access, 10, 51922-51950.

[2] Chang, T. Y., & Chiang, H. T. (2025). An Innovative Transformation Assessment Model for High-altitude Operations Based on Multi-dimensional Indicator System. Advances in Management and Applied Economics, 15(2), 1-8.

[3] Li, X., Ke, Z., Huang, Y., Chen, M., & Chen, Z. (2024, September). Research on Proactive Safety Pre-Control Device for High-Altitude Workers in Power Grid to Prevent Falling. In 2024 3rd International Conference on Artificial Intelligence and Computer Information Technology (AICIT) (pp. 1-4). IEEE.

[4] Spertino, F., & Corona, F. (2013). Monitoring and checking of performance in photovoltaic plants: A tool for design, installation and maintenance of grid-connected systems. Renewable Energy, 60, 722-732.

[5] Wang, Z., Ou, Y., Li, H., Zeng, W., Gao, Q., Zou, Y., & Li, P. (2021, June). High-altitude fall prevention method and device for power transmission line. In IOP Conference Series: Earth and Environmental Science (Vol. 791, No. 1, p. 012095). IOP Publishing.

[6] Haoyu, S., Tianqi, L., Tao, B., Chuan, H. E., Yue, Y. I. N., & Lijie, D. I. N. G. (2020). Operational risk assessment of power system considering wind power and photovoltaic grid connection. Modern Electric Power, 37(4), 358-367.

[7] Euler, S., Lin, X., Tejedor, E., & Obregon, E. (2022). High-altitude platform stations as international mobile telecommunications base stations: A primer on HIBS. IEEE Vehicular Technology Magazine, 17(4), 92-100.

[8] Yuan, S., & Chen, C. (2024). A Latest Equipment for Safe High-Altitude Operations. International Journal of New Developments in Engineering and Society, 8(5).

[9] Mao, X., Zhang, Y., Wang, Z., Pan, W., Zhang, W., Wang, J., ... & Hu, X. (2020). Design of rescue equipment for high altitude electrical operation. In IOP Conference Series: Materials Science and Engineering (Vol. 740, No. 1, p. 012108). IOP Publishing.

[10] Zhan, P., Zeng, Y., & Yu, S. (2024, November). Research on fall prevention and safety protection for electric power tower climbing operations based on the longhorn whisker algorithm. In Journal of Physics: Conference Series (Vol. 2876, No. 1, p. 012016). IOP Publishing.

[11] Ma, A., Weng, X., Chen, Y., Xu, W., Liang, C., Dong, J., & Hu, Z. (2023, November). Smart belt for real-time posture monitoring of grid workers at heights. In 2023 IEEE Sustainable Power and Energy Conference (iSPEC) (pp. 1-5). IEEE.

[12] Zhou, Q., & Liu, D. (2024). Improving safety in high-altitude work: semantic segmentation of safety harnesses with CEMFormer. Symmetry, 16(11), 1449.

[13] Kong, C., Chen, B., Wang, L., Hu, J., & Wei, J. (2025, May). Research on the application of double buckle safety fall protection device in transmission line tower climbing operation. In Journal of Physics: Conference Series (Vol. 3011, No. 1, p. 012048). IOP Publishing.

[14] Li, L., Ren, P., Sun, H., Shan, Z., Yang, S., Liu, S., & Song, T. (2022, April). Fall prevention steering gear for high-altitude operation. In 2nd International Conference on Mechanical, Electronics, and Electrical and Automation Control (METMS 2022) (Vol. 12244, pp. 253-258). SPIE.

[15] Hu, Z., He, G., Zhang, X., Huang, T., Li, H., Zhang, Y., ... & Ning, F. (2023). Impact behavior of nylon kernmantle ropes for high-altitude fall protection. Journal of Engineered Fibers and Fabrics, 18, 15589250231167401.

[16] Zhang, P., Ma, L., Sun, F., Ma, Y., Zhu, K., & Jia, S. (2023, December). Research on Near-Electric Warning Method of High-Altitude Construction Machinery. In 2023 5th International Academic Exchange Conference on Science and Technology Innovation (IAECST) (pp. 1125-1128). IEEE.